CHEMISTRY OF MATERIALS

pubs.acs.org/cm

Article

High-Purity, High-Yield Synthesis of Covalent Organic Framework Nanosheets for Fast and Selective Molecular Separation

Zhipeng Zhang,[§] Qianqian Lan,[§] Decai Liao, Xiansong Shi,* Mingjie Wei, Zhe Zhang, Xingyuan Wang, and Yong Wang*

Cite This: *Chem. Mater.* 2022, 34, 6345−6354

Read Online

ACCESS | Metrics & More | Article Recommendations | Supporting Information

ABSTRACT: Covalent organic framework nanosheets (CONs) with extremely thin thicknesses and inborn penetrating nanopores are attractive in transport-related applications. However, the strong tendency of $\pi-\pi$ stacking between adjacent laminates hinders their mass production. Herein, we report a facile glycerol-mediated strategy for synthesizing various well-dispersed CONs in liquid phases. The CONs are readily prepared by dissolving monomers in glycerol and subsequent thermal condensation. Experimental and computational investigations reveal that the strong hydrogen bonds between glycerol and CONs suppress the $\pi-\pi$ stacking interaction, leading to well-dispersed CONs. Additionally, glycerol acetalization with aldehyde monomers also contributes to the formation of CONs by decreasing the diffusion rate of reactants. The synthesized CONs show a lateral size of over 10 μm and a uniform thickness of ∼4 nm, and their yield is as high as ∼73%. CONs deposited on porous substrates exhibit remarkable permselectivities surpassing most reported membranes and exceptional dye/salt separation performances. This study provides a new strategy for synthesizing CONs and increases the understanding of the important role of solvents in the synthesis of two-dimensional materials.

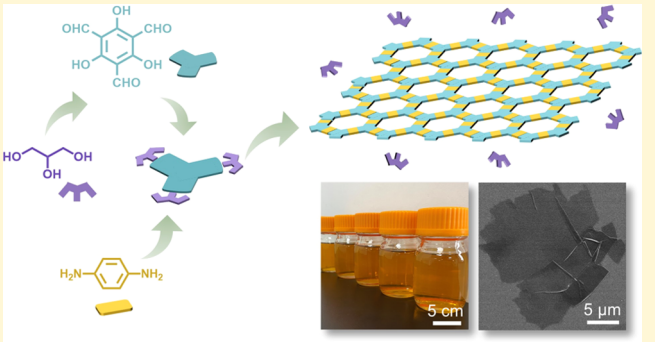

1. INTRODUCTION

Two-dimensional (2D) covalent organic frameworks (COFs) are porous crystalline polymers with inborn nanopores and laminated structures integrated by in-plane covalent bonds and interlamellar van der Waals (vdW) forces.[1−3] By conquering the interlamellar interactions, COF nanosheets (CONs) with infinitesimal thicknesses can maximize the potential of COFs.[4,5] As an emerging 2D porous nanostructure, CONs highlighted with an ultrathin thickness, penetrating nanoporosity, and good thermal/chemical stability have shown great potential in a diversity of applications ranging from catalysis to optoelectronics and to molecular separation.[6−9]

Since the first report of CONs in 2007,[10] significant efforts have been made to synthesize CONs, and the reported synthetic routes can be generally classified into the "top-down" and "bottom-up" processes. The "top-down" strategy relies on mechanical or chemical exfoliation of COF bulks into single- or few-layered 2D structures. Typical methods include sonication,[11] mechanical grinding,[12] and chemical intercalation.[13] Unfortunately, the CONs produced by these exfoliation methods usually suffer from structural defects and damages, inhomogeneous thicknesses, and low yields. To cope with these limitations, the "bottom-up" strategy with the advantage of directly forming large-area and high-quality CONs has been developed. For example, the introduction of a third monomer with large rigid groups at the edge of CONs *via* imine exchange can enlarge the distance between the adjacent frameworks, allowing anisotropic growth along the planar directions to form ultrathin CONs.[14] Another route is to grow CONs on solid surfaces followed by detaching the CONs from the substrates. Salt crystals as the soluble template can provide rich solid−liquid interfaces in reaction systems, inducing the interface-confined synthesis of few-layered CONs.[15] However, the use of these organic and inorganic auxiliaries or additives inevitably causes the hassle of additional operations and impurities, which not only complicates the synthesis but also debases the CON quality and purity. Therefore, it remains highly demanding for synthetic routes capable of facilely and massively producing high-quality CONs.

Recently, noncovalent interactions have been proved to play a vital role in the initial self-assembly of COF nanostructures.[16] This provides a potential opportunity to synthesize CONs by carefully controlling the solvent environment. Although the

Received: March 19, 2022
Revised: July 3, 2022
Published: July 14, 2022

https://doi.org/10.1021/acs.chemmater.2c00834
Chem. Mater. 2022, 34, 6345−6354

influence of solvents on the dimensional parameters of COFs remains to be elucidated, the solvent should be able to weaken the $\pi-\pi$ interactions, thus suppressing the $\pi-\pi$ stacking-induced aggregation of 2D conjugated oligomers that are polymerized from monomers and facilitating the lateral growth of freestanding CONs. Glycerol, with the strong hydrogen-bond forming capability and high viscosity because of the presence of high-density hydroxyl groups, can decrease the diffusion rate of reactants and change the reaction kinetics and consequently the morphology of products.[17,18] As a result, glycerol has been used in the synthesis of low-dimensional inorganic nanostructures, such as nickel oxide (NiO) nanobelts[19] and titanium oxide (TiO_2) nanosheets.[20] Very recently, we used glycerol as the solvent to synthesize phenolic nanomeshes by driving the precursor micelles to assemble and polymerize exclusively in the lateral direction.[21] Considering the intrinsic 2D layered structure of COFs, we envision that applying glycerol as the synthesis medium is likely to inhibit the axial $\pi-\pi$ stacking of the COF primary structures and simultaneously promote their lateral growth, thus enabling the *in situ* formation of uniform and ultrathin CONs. In this process, no additives are involved and the monomers can be efficiently transformed into CONs, ensuring a high purity and high yield of CONs.

Herein, we report a glycerol-mediated strategy for the facile production of high-quality CONs in the liquid phase. The acetalization between glycerol and aldehyde together with a high-viscosity environment slows down the condensation reaction, which leads to the generation of CONs with the aid of hydrogen bonds in glycerol. This strategy enables the universal synthesis of CONs with different structures and linkages. Further, we demonstrate that the synthesized CONs can be deposited on macroporous substrates to prepare high-flux membranes with a sharp selectivity enabling effective dye/salt separation.

2. EXPERIMENTAL SECTION

2.1. Materials. 1,3,5-Triformylphloroglucinol (Tp, 98%), 1,3,5-triformylbenzene (Tb, 98%), and 1,4-phenyldiboronic acid (98%) were provided by Jilin Chinese Academy of Sciences—Yanshen Technology Co., Ltd. *p*-Phenylenediamine (Pa, 99%), 4,4′-diaminobiphenyl (BD, 98%), and hydrazine hydrate (Hz, 98%) were purchased from Aladdin. 3,3′-Dihydroxybenzidine ($BD(OH)_2$, 99%) was purchased from TCI. Congo red (CR) and acid fuchsin (AF) were supplied by the Tianjin Institute of Chemical Reagent. Inorganic salts, glycerol (99%), and other solvents all of analytical grade were obtained from local suppliers. All chemicals were used as received. Porous anodic aluminum oxide (AAO) disks (diameter: 2.5 cm, Whatman) with a nominal pore size of 100 nm were used as the support. Deionized water (conductivity: 2−10 $\mu S\ cm^{-1}$) was used in all of the experiments.

2.2. Glycerol-Mediated Synthesis of CONs. CONs were *in situ* synthesized in glycerol. Taking the synthesis of TpPa nanosheets as an example, 0.03 mmol of Tp (6.3 mg) and 0.045 mmol of Pa (4.8 mg) were separately dissolved in 15 mL of glycerol and then mixed together by stirring at 300 rpm for 30 min. Subsequently, 0.5 mL of acetic acid was added to the mixture. After stirring for ∼2 h to form a homogeneous solution, the solution was transferred to a Schlenk tube, degassed, and then left undisturbed at 120 °C to perform thermal treatment for 3 days. Finally, TpPa nanosheets were produced in the form of a dispersion in glycerol with a concentration of 273 mg L^{-1}. TpPa nanosheets were also synthesized with double (0.06 mmol of Tp and 0.09 mmol of Pa) and triple (0.09 mmol of Tp and 0.135 mmol of Pa) monomer concentrations with other conditions unchanged.

Other imine-linked CONs were synthesized by replacing the corresponding aldehyde and amine monomers and maintaining other conditions unchanged. Boron-containing COF-1 nanosheets were synthesized by directly dissolving 0.06 mmol of 1,4-benzenediboronic acid (9.9 mg) in 15 mL of glycerol, followed by transferring to a Schlenk tube, degassing, and thermal treatment as above.

2.3. Synthesis of TpPa in Various Solvents. In addition, we also synthesized TpPa using ethanol and glycerol/ethanol mixtures with glycerol proportions of 33, 50, 66, 90, and 97% in volume as the solvents for comparison. Glycerol was also replaced by isopropanol, ethylene glycol, poly(ethylene glycol) with a molecular weight of 400 Da (PEG-400), and poly(propylene glycol) with a molecular weight of 8000 Da (PPG-8000) to synthesize TpPa with other conditions unchanged.

2.4. Preparation of CON Membranes. In a typical membrane preparation process, as-synthesized CON dispersions were diluted with ethanol. The CON membranes were prepared by depositing the diluted dispersions onto AAO supports by vacuum filtration at a relatively low pressure of 5 kPa, followed by continuous filtration of abundant ethanol to remove the residual glycerol. The obtained CON membranes were dried at room temperature for the following characterizations and performance evaluations. The membranes with different deposition densities were obtained by changing the volume of CON dispersions.

2.5. Simulations. All of the molecular dynamics (MD) simulations were performed by the large-scale atomic/molecular massively parallel simulator (LAMMPS) package. We specified the polymer consistent force field (PCFF) in all simulations, which has been widely adopted for small organic molecule and polymer simulations.[22] The interactions of all atoms were described by Lennard-Jones (LJ, 9-6) and Coulombic potentials. The cutoff distances of LJ and Coulombic potentials were set as 1.2 nm. Three-dimensional periodic boundary conditions (PBC) were applied to avoid the influence of the box boundary during simulation. Initial solution models for molecular dynamics simulations were constructed by the Packmol software package. The simulations were carried out under the NVT canonical ensemble for 10 ns at 393.15 K. The nonbond energy was calculated in accordance with the following equation

$$E = E_{vdW} + E_{coulomb}$$

The nonbond energy comprises LJ (9-6) van der Waals (vdW) and Coulombic interactions.

2.6. Characterizations. Field-emission scanning electron microscopy (SEM) images were obtained on a Hitachi S4800 microscope at an accelerating voltage of 3 kV. All samples were ion-sputtered with a thin layer of gold to enhance the conductivity before observations. High-resolution transmission electron microscopy (HRTEM) images were taken on a JEOL JEM-2100 microscope operated at a voltage of 200 kV. Atomic force microscopy (AFM) measurements were performed on an XE-100 instrument (Park Systems) under a noncontact mode. Fourier transform infrared (FTIR) spectra were obtained using a spectrometer (Nicolet 8700) in the scanning range of 4000−400 cm^{-1}. ^{13}C solid-state nuclear magnetic resonance (NMR) was taken on a Bruker 400M NMR spectrometer. X-ray diffraction (XRD) patterns were recorded on a Smart Lab X-ray diffractometer (Rigaku, Cu Kα radiation, λ = 0.15418 nm) with a 2θ range of 2−30°, and the scanning step was 0.02° s^{-1}. ^1H NMR data were measured using a JEOL JNM-ECZ400S NMR spectrometer using deuterated dimethyl sulfoxide (DMSO) as the solvent. As the amount of Tp in the synthesis of CONs is too low to be detected, the ^1H NMR measurement was conducted on the Tp/glycerol mixture, in which the Tp amount is 1000 times higher than the original value; 5 mg of Tp and 15 mg of glycerol were predissolved in 0.25 mL of deuterated DMSO, respectively. Then, the two were mixed and transferred to an NMR tube to monitor their reaction at 0 and 72 h. Electrospray ionization mass spectra (ESI-MS) were collected on an Agilent 1260 HPLC-6500 Q-TOF mass spectrometer. The viscosity of glycerol/ethanol mixtures with different glycerol proportions was measured by a DV2T rotational viscometer (Brookfield) at 25 °C.

https://doi.org/10.1021/acs.chemmater.2c00834
Chem. Mater. 2022, 34, 6345−6354

Scheme 1. Schematic Illustration of the Glycerol-Mediated Synthesis of TpPa Nanosheets

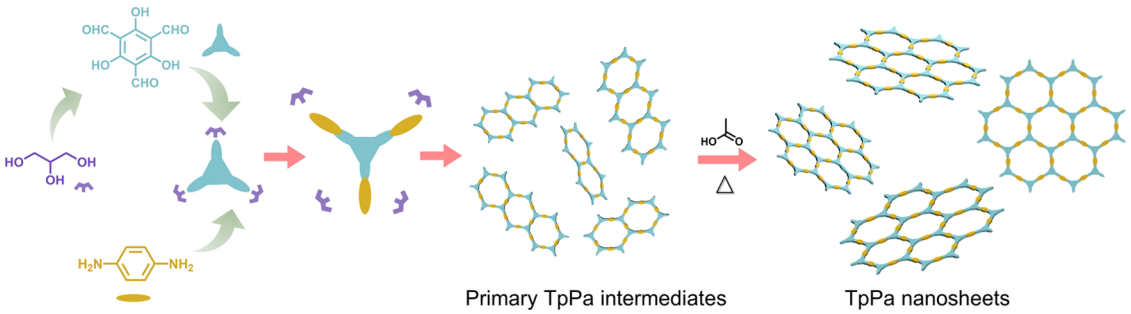

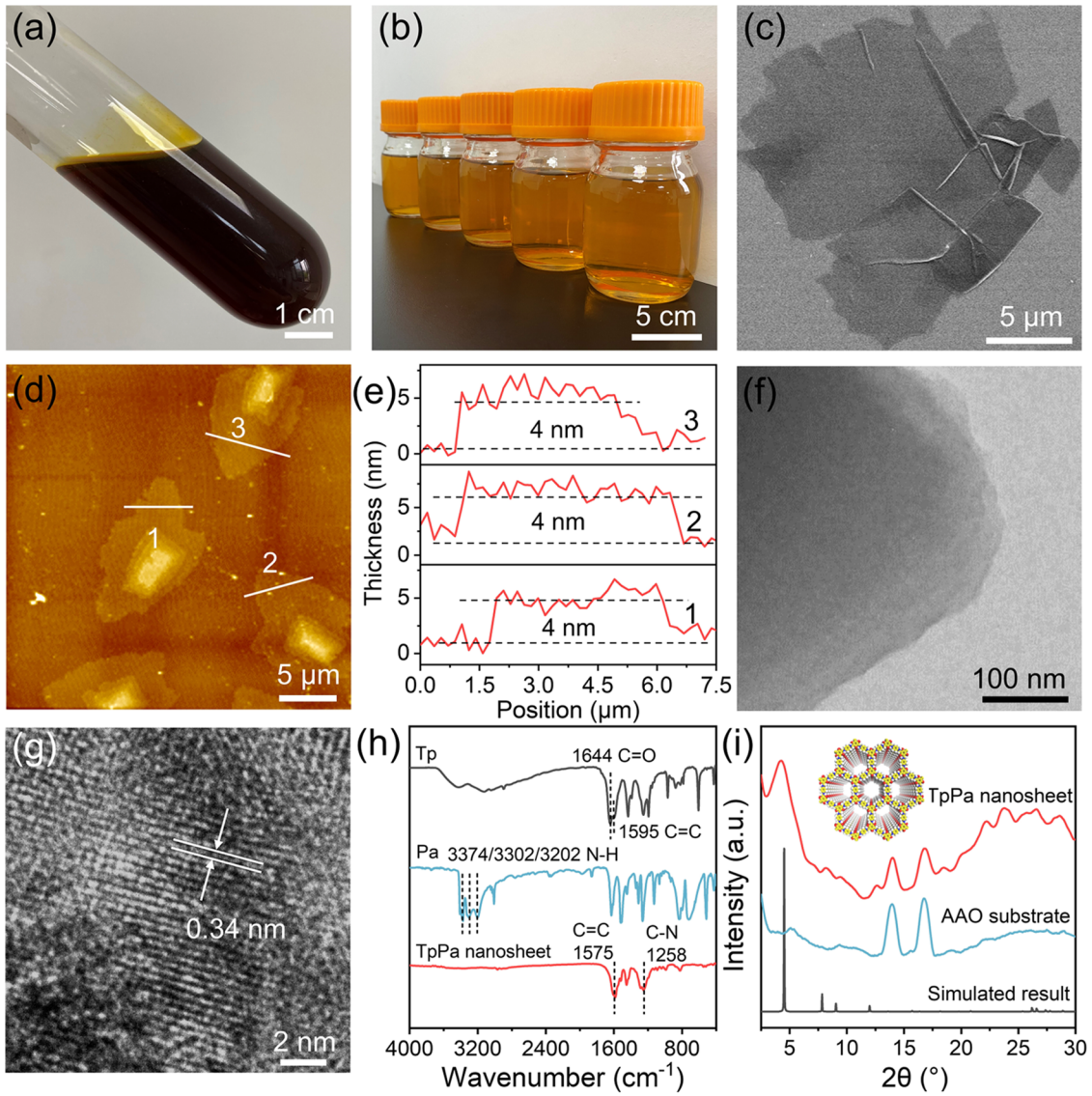

Figure 1. Characterization of TpPa nanosheets. Photographs of the TpPa nanosheet dispersions (a) after thermal treatment and (b) further diluted with ethanol. (c) SEM image, (d) AFM image, and (e) the corresponding height profiles. (f) Low-magnification and (g) high-magnification TEM images. (h) FTIR spectra of the Tp, Pa, and TpPa nanosheets. (i) XRD patterns of the AAO substrate, TpPa nanosheets collected on the AAO substrate, and simulated TpPa with an eclipsed stacking model. The inset in (i) is the structural diagram of TpPa.

The surface ζ potentials of membranes were analyzed by an electrokinetic analyzer (SurPASS, Anton Paar GmbH) with a streaming potential method; 1 mmol L^{-1} KCl aqueous solution was used as the background electrolyte solution.

2.7. Filtration Tests. Separation performances of the prepared CON membranes including water permeances and rejection rates to salts and dyes were examined using a dead-end filtration cell (Amicon 8003, Millipore) under a pressure of 0.6 bar. Before the tests, the membranes were prepressed at 0.6 bar for 10 min to ensure a steady permeation. The aqueous solutions of CR (50 ppm), AF (25 ppm), and inorganic salts (1000 ppm) were used as the feed solutions for rejection tests. The concentrations of the salt solutions before and

https://doi.org/10.1021/acs.chemmater.2c00834
Chem. Mater. 2022, 34, 6345−6354

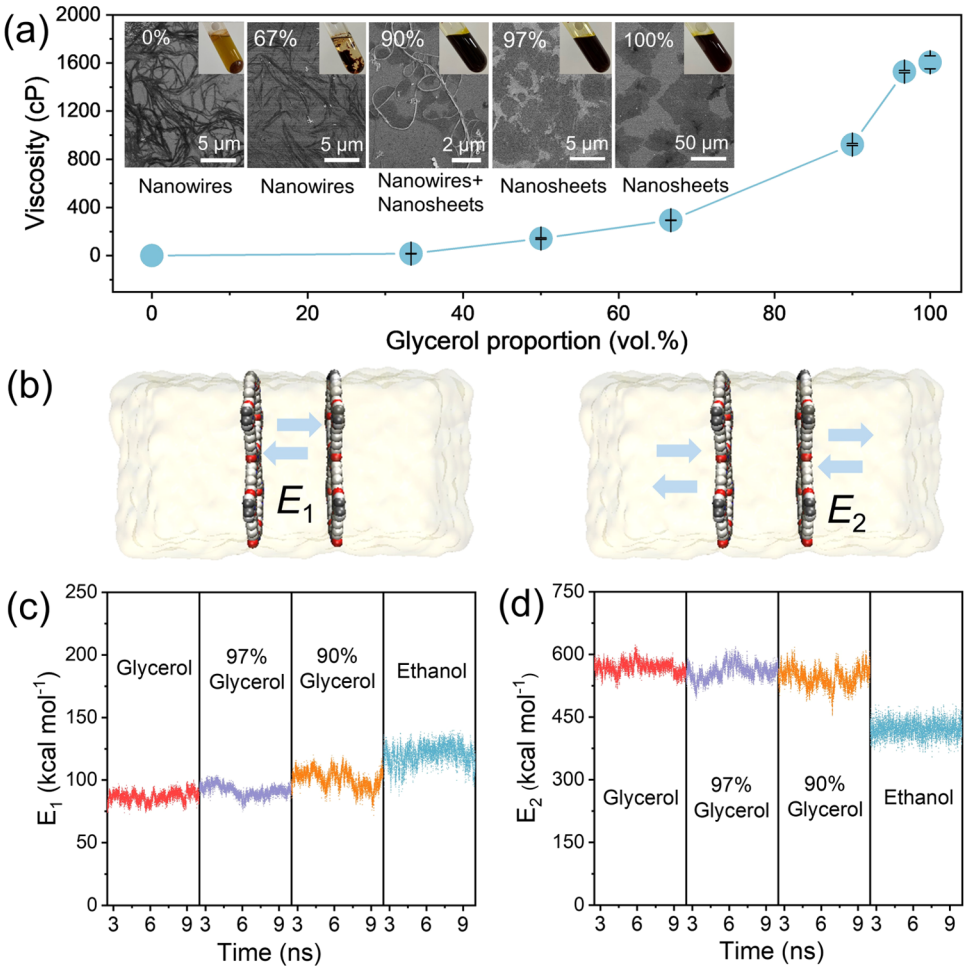

Figure 2. Mechanism understanding of the formation of TpPa nanosheets. (a) Viscosity variation of glycerol/ethanol mixtures with an increasing proportion of glycerol. Insets in panel (a) are the corresponding photographs and SEM images of TpPa products. (b) Schematic diagram of MD simulations on the microscopic motion of TpPa in the solvent. (c) Interaction energy between two TpPa monolayers (E_1). (d) Interaction energy between the TpPa monolayer and solvent (E_2).

after the filtration were measured using a conductivity meter (S230-K, Mettler Toledo). The concentrations of dyes in the feed and permeate were determined with a UV−vis spectrophotometer (NanoDrop 2000C, Thermo Fisher Scientific). The pure water permeance (PWP, L m^{-2} h^{-1} bar^{-1}) and rejection rates (R, %) of membranes were calculated as follows

$$\mathrm{PWP} = V/(A\Delta tP) \quad (1)$$

$$R = (1 - C_P/C_F) \times 100\% \quad (2)$$

where V (L) is the water volume passing through the membrane, A (m^2) is the effective area of the membrane, Δt (h) is the filtration time, and P (bar) is the testing pressure. C_P and C_F (g L^{-1}) are the concentrations of permeation and feed solutions, respectively.

Dye/salt separation performances were evaluated by filtering the mixture of NaCl (1000 ppm) and CR (50 ppm). The concentrations of NaCl were tested by ion chromatography (ICS 2000, Thermo Fisher Scientific) after the complete adsorption of CR using activated carbon.

3. RESULTS AND DISCUSSION

3.1. Glycerol-Mediated Synthesis of TpPa Nanosheets. The synthesis of TpPa nanosheets starts with mixing of the monomer pairs predissolved in glycerol to form TpPa intermediates, followed by thermal treatment at 120 °C for 3 days to ensure adequate condensation and crystallization (Scheme 1). In sharp contrast to the aggregation and sedimentation of TpPa products in conventional syntheses,[23] herein the reaction system remains homogeneous without precipitates during the entire synthesis (Figures 1a and S1). The darkening color of the TpPa dispersion indicates the proceeding of the condensation reaction in the thermal treatment. The obtained homogeneous TpPa dispersion remains stable for at least 3 months. As the glycerol-mediated synthesis is extremely simple and requires no adjuvants, a large volume of TpPa dispersions can be obtained by diluting the as-synthesized sample, which remain stable for weeks (Figure 1b). The excellent dispersity and stability should be attributed to the fact that glycerol is able to form strong hydrogen bonds with aldehyde and amine groups carried on the monomers, intermediates, as well as the nanosheets, thus preventing the $\pi-\pi$ stacking between them.

The structural features of the produced TpPa nanosheets were studied by SEM and AFM after depositing the diluted TpPa dispersion on silicon wafers. As shown in Figures 1c and S2, the obtained TpPa products are exclusively in the form of thin sheets without the interference of any other morphologies. The sheets exhibit a well-defined 2D structure with lateral sizes of up to >10 μm. AFM analysis reveals that the TpPa sheets possess a lamellar structure with a thin and uniform thickness of ~4 nm (Figure 1d,e). That is, the TpPa nanosheets are

https://doi.org/10.1021/acs.chemmater.2c00834
Chem. Mater. 2022, 34, 6345−6354

directly produced in glycerol without any postsynthetic delamination processes. The TEM image in Figure 1f further substantiates the low thickness of TpPa nanosheets. Moreover, the high-resolution TEM image (Figure 1g) shows that the TpPa nanosheets are crystallized with an interlayer distance of ~0.34 nm indexed to the (001) lattice plane.[24] By comparing the mass of the collected nanosheets and the raw materials, we recognize a nanosheet yield as high as ~73%. Thus, applying glycerol as the solvent enables the single-step synthesis of high-quality TpPa nanosheets with a high yield.

As shown in Figure 1h, Tp and Pa show characteristic peaks at 1644 cm^{-1} (stretching vibrations of C═O) and 3374−3202 cm^{-1} (stretching vibrations of N−H), respectively. These peaks disappear in the spectrum of TpPa nanosheets, suggesting the complete consumption of monomers. Meanwhile, two new peaks at 1575 and 1258 cm^{-1} are observed, which can be attributed to the stretching vibrations of C═C and C−N, indicating the formation of β-ketoenamine TpPa.[25] The β-ketoenamine structure is additionally confirmed by ^{13}C cross-polarization magic-angle-spinning (CP-MAS) solid-state NMR spectroscopy, with the presence of the carbon signals in C═O, C═C, and C−N at 183.1, 147.3, and 135.7 ppm, respectively (Figure S3). We then investigated the crystallinity of TpPa nanosheets by XRD characterization (Figure 1i). The peaks at 2θ values of 14 and 17° are assigned to the AAO support. The TpPa nanosheets exhibit a distinct peak at 4.7° and a broad peak at 27°, which is in agreement with the simulated pattern in the eclipsed stacking mode. Specifically, the two peaks correspond to the (100) and (001) crystal facets, respectively, confirming the successful formation of crystalline TpPa nanosheets.[26]

3.2. Mechanism Understanding of the Formation of TpPa Nanosheets. It has long been reported that glycerol may react with aldehydes *via* acetalization.[27,28] Therefore, we first check the possibility of acetalization between glycerol and Tp in the present work to reveal the formation mechanism of TpPa nanosheets. There is an obvious decrease in the relative content of Tp in the ^1H NMR spectra after mixing Tp and glycerol at room temperature for 72 h (Figure S4). Meanwhile, the mass spectroscopy analysis shows the disappearance of Tp after thermal heating at 120 °C, accompanied by the formation of species with higher molecular weights (Figure S5). These results clearly confirm the occurrence of acetalization. It is worth noting that acetalization is highly reversible,[29] which only slows down the condensation reaction between Tp and Pa, thus contributing to the formation of TpPa nanosheets.[14]

We then monitored the growth process of TpPa nanosheets. When the monomers are mixed and stirred for a few minutes, the primary TpPa intermediates in the elongated leaflike architecture with a length of several micrometers and a thickness of 3−4 nm are formed (Figure S6). After adding the catalyst and further stirring for 2 h, large-size nanosheets are obtained (Figure S7). Notably, the ultimate TpPa nanosheets are unchanged in thickness but enlarged in lateral size compared with the primary TpPa intermediates. This indicates that TpPa nanosheets are exclusively formed by the horizontal assembly of primary TpPa intermediates in the absence of vertical stacking. The monomer concentration plays an important role in the production of high-quality CONs. We doubled and tripled the concentrations of both Tp and Pa and maintained other conditions unchanged to synthesize TpPa. The obtained COF products in both cases retain the morphology of nanosheets; however, they show a tendency to aggregate because of higher concentrations of TpPa nanosheets formed in the dispersion of glycerol as a result of the higher monomer concentrations (Figure S8).

Further, to verify the irreplaceable role of glycerol, we investigated the morphologies of TpPa products synthesized using glycerol/ethanol mixtures with varied glycerol proportions as the synthesis solvent. Considering the high viscosity of glycerol, we associated the viscosities of the glycerol/ethanol mixtures with the glycerol proportions for investigation. As shown in Figure 2a, the mixtures with glycerol proportions lower than 67% exhibit viscosities of below 400 cP, which are greatly increased to over 1500 cP when the glycerol proportions are higher than 97%. The photographs and SEM images of TpPa products synthesized in mixtures with varied glycerol proportions are shown in the inset of Figure 2a. Visible precipitates are formed when the glycerol proportion is lower than 67%, while the glycerol proportions higher than 90% lead to homogeneous dispersions. Meanwhile, the TpPa products undergo a morphology transformation from nanowires to nanosheets with increasing glycerol proportions. These results indicate that a high-viscosity environment is beneficial to the dispersity of products and the formation of well-defined nanosheets. Notably, the nanosheets synthesized in the mixture with 97% glycerol are in the thickness of 5−6 nm (Figure S9), which is thicker than those synthesized in pure glycerol. In addition, when glycerol is replaced by other hydroxyl-containing solvents (*i.e.*, isopropanol, ethylene glycol, PEG-400, and PPG-8000), sheetlike structures are not produced at all (Figure S10), demonstrating the irreplaceability of glycerol. Considering the fact that the highly viscous PEG-400 and PPG-8000 carry much fewer hydroxyl groups than glycerol, we reason that the hydrogen-bond interaction plays a critical role in forming well-dispersed CONs. Moreover, when adding ethanol into the as-synthesized CON dispersion to weaken the hydrogen bonds, we observe a significant aggregation of these CONs, confirming the importance of strong hydrogen-bond interactions for the formation of CONs (Figure S11).

To gain more insights into the formation mechanism, we carried out MD simulations to study the interactions between related components in different solvent systems.[30] The intermolecular interaction energy between two adjacent TpPa monolayers (E_1) and the energy of the TpPa monolayer toward the solvent (E_2) were calculated to demonstrate how glycerol affects the axial interaction of COF monolayers to form nanosheets (Figure 2b). A low E_1 and high E_2 are preferential to form well-defined nanosheets. As shown in Figure 2c, the introduction of glycerol obviously weakens E_1 in the glycerol/ethanol system, thus inhibiting the $\pi-\pi$ stacking of TpPa monolayers. Moreover, E_1 in glycerol (86 kcal mol^{-1}) is much lower than E_1 in 1,4-dioxane (152 kcal mol^{-1}, Figure S12), which could be the reason for the structural difference of final products. In addition, Figure 2d exhibits that E_2 in glycerol (569 kcal mol^{-1}) is much higher than E_2 in ethanol (421 kcal mol^{-1}) and E_2 in 1,4-dioxane (306 kcal mol^{-1}, Figure S12), revealing the stronger affinity of TpPa toward glycerol. Particularly, there is a 6-fold energy difference between E_1 in glycerol and E_2 in glycerol, which clearly demonstrates the strong interactions of glycerol toward TpPa. Moreover, these simulation results are in good agreement with the experimental results discussed above, revealing the importance of the solvent to the morphology of final products.

https://doi.org/10.1021/acs.chemmater.2c00834
Chem. Mater. 2022, 34, 6345−6354

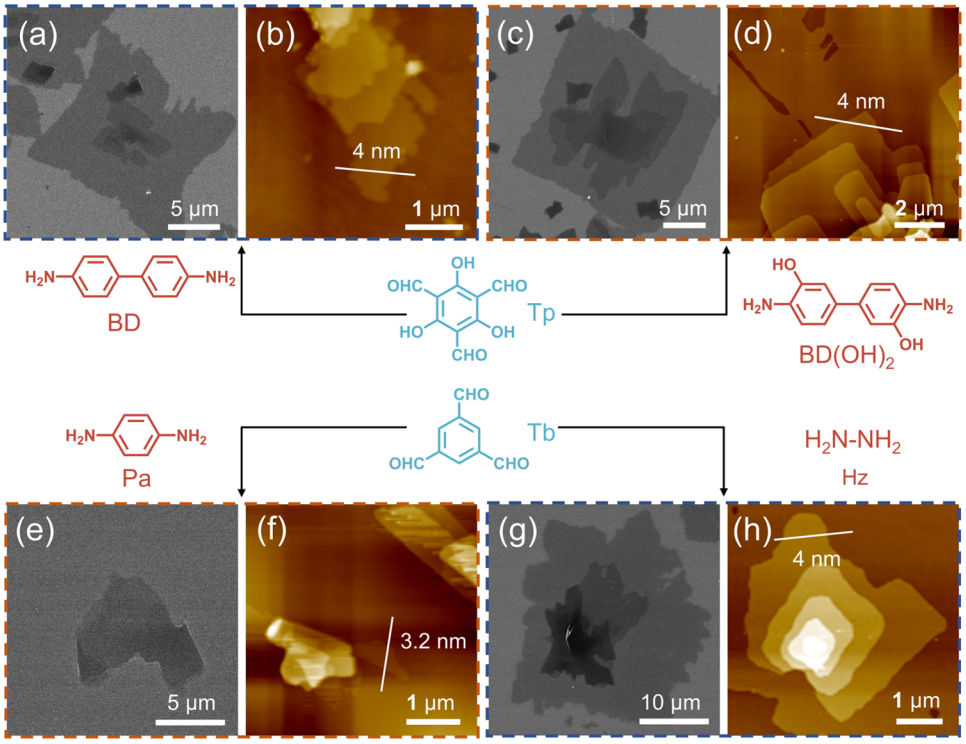

Figure 3. Scheme of the synthesis of various CONs and (a, c, e, g) SEM and (b, d, f, h) AFM images of the synthesized TpBD, TpBD(OH)$_2$, COF-LZU1, and ACOF-1 nanosheets.

Based on the above experimental observations and simulated results, we disclose the process of glycerol-mediated synthesis of TpPa nanosheets as follows: first, the acetalization and high-viscosity environment collectively slow down the rate of the condensation reaction between Tp and Pa. Then, the strong interactions between glycerol and monomers as a result of hydrogen bonds suppress the interlayer $\pi-\pi$ interactions and thereby promote the polymerization reactions along the 2D direction, leading to the formation of well-dispersed nanosheets rather than aggregated bulks. In the whole synthesis, glycerol plays multiple roles and serves as the solvent, dispersant, mediator, and stabilizer, which is irreplaceable in the formation of TpPa nanosheets. With the particular environment of high viscosity, strong glycerol−TpPa interactions, and weakened $\pi-\pi$ stacking interactions, TpPa nanosheets are directly synthesized and *in situ* dispersed in glycerol.

3.3. Synthesis of Other CONs by Glycerol-Mediated Synthesis. In view of the simplicity and repeatability of the glycerol-mediated synthesis, other CONs prepared from monomer pairs soluble in glycerol are expected to be achieved. We synthesized several β-ketoenamine and imine-linked CONs including TpBD,[31] TpBD(OH)$_2$,[32] COF-LZU1,[33] and ACOF-1[34] nanosheets and further confirmed their 2D structure by SEM and AFM. As shown in Figure 3a−d, TpBD and TpBD(OH)$_2$ nanosheets were fabricated by separately employing BD and BD(OH)$_2$ to replace Pa as the amine building blocks. The resulting products are macroscopically well dispersed in glycerol (Figure S13a,b) and microscopically display well-defined sheetlike morphologies with lateral sizes larger than 10 μm and uniform thicknesses of ∼4 nm. Additionally, the same synthesis procedure was carried out by replacing Tp with Tb as the aldehyde monomer and homogeneous COF-LZU1 and ACOF-1 nanosheet dispersions were accordingly obtained (Figure S13c,d). Figure 3e−h reveals the micron-sized nanosheet morphologies of COF-LZU1 and ACOF-1 with thicknesses of ∼3.2 and ∼4 nm, respectively. Therefore, a series of thin and uniform CONs can be synthesized from diverse monomers, proving the universality of the glycerol-mediated synthesis. The similar thickness of these CONs is possibly because the monomers are analogous in groups, leading to similar solvent−CON and CON−CON interactions. Therefore, by regulating the molecular structures of monomers, CONs with further tailored thicknesses are expected to be achieved. Taking the boron-containing COF-1 as an example, the self-condensation of 1,4-benzenediboronic acid in glycerol produces thin nanosheets with only 2 nm in thickness (Figure S14). This result further indicates the universality of our method toward synthesizing CONs with diverse linkages. In addition to COF nanosheets, the glycerol-mediated strategy proposed in this work is expected to be generally applicable for the synthesis of other framework nanosheets if their formation is controlled by the diffusion of monomers or precursors in liquids.

3.4 Preparation and Separation Performance of CON Membranes. Two-dimensional materials featuring ultrathin thicknesses have shown remarkable advantages for building separation membranes.[35,36] We constructed TpPa nanosheet separation layers on AAO supports by vacuum filtration to prepare TpPa membranes.[37] The bare AAO substrate is white in color and it turns deep red after depositing TpPa nanosheets (Figure 4a). The SEM image of the AAO support shows large pores with a diameter of ∼100 nm (Figure S15). These large pores are then covered with a continuous selective layer assembled by TpPa nanosheets (Figure 4b). We checked the cross-sectional morphology of these membranes. As shown in Figure 4c, a deposition density of 52 μg cm^{-2} produces a TpPa layer with a thickness of ∼1.4 μm. Other membranes produced

https://doi.org/10.1021/acs.chemmater.2c00834
Chem. Mater. 2022, 34, 6345−6354

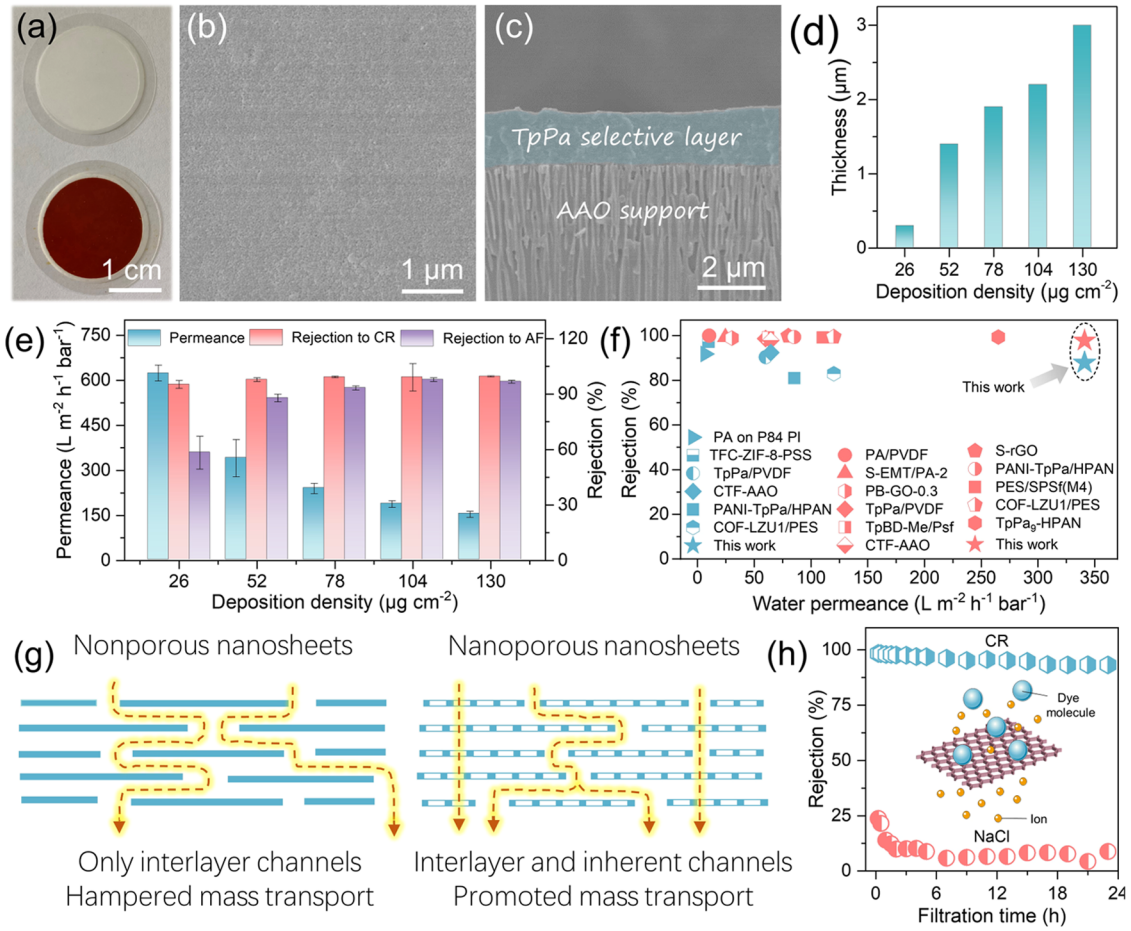

Figure 4. Characterizations and separation performances of TpPa membranes. (a) Photographs of the AAO support (up) and TpPa membrane with a deposition density of 52 μg cm^{-2} (down). (b) Surface and (c) cross-sectional SEM images of the TpPa membrane with a deposition density of 52 μg cm^{-2}. The TpPa nanosheet layer was false-colored. (d) Thickness of the nanosheet layer as a function of the deposition density. (e) Water permeances and dye rejections. (f) Comparison of the separation performance between our TpPa membrane and other membranes (red code: Congo red; blue code: acid fuchsin). (g) Schematic diagram of the water transport pathways in porous and nonporous nanosheet membranes. (h) Rejection to CR and NaCl in a long-time separation of the mixture using the TpPa membrane prepared with a deposition density of 78 μg cm^{-2}. The inset in (h) is the schematic diagram of the separation process.

under various deposition densities present similar surface morphologies and different cross-sectional thicknesses as shown in Figures S16 and S17. All of these membranes show continuous TpPa layers tightly attached to the AAO substrate. In Figure 4d, the thickness of the deposited nanosheet layer is linearly increased with the raised deposition density and can be tuned in the range of 0.3−3.2 μm by simply changing the volume of the deposited TpPa nanosheet dispersion. Moreover, this linear adjustability of the thickness illustrates an excellent homogeneity of the nanosheet dispersion, which benefits the design of nanosheet layers with desired thicknesses.[38] Therefore, through a facile vacuum filtration process, we realize the controllable preparation of CON membranes. The prepared membranes hold a composite structure with the nanosheet-stacked layers serving as the separation layer for selective passage of solutes, promising a desirable selectivity by the size-dependent exclusion.

To assess the separation performances of the obtained CON membranes, the pure water permeances and rejections to two dyes, CR and AF (detailed information is given in Table S1), were tested.[39] The relationship between the separation performances of TpPa membranes and the deposition densities of nanosheets is shown in Figure 4e. Under a low deposition density of 26 μg cm^{-2}, the TpPa membrane exhibits a high permeance of ~624 L m^{-2} h^{-1} bar^{-1} and a considerable CR rejection of ~95.3%. A further increase in the deposition density leads to continuously decreased water permeance, finally achieving a permeance of ~154 L m^{-2} h^{-1} bar^{-1} at 130 μg cm^{-2}. Meanwhile, the CR rejection is slightly increased to ~99.6%. In the case of AF, the rejection is gradually enhanced from ~58.3 to ~96.8% with the increased deposition density from 26 to 130 μg cm^{-2}. We note that the adsorption of dye molecules by TpPa nanosheets can be neglected, as confirmed by the UV−vis absorption spectra of the feed, filtrate, and retentate (Figure S18). Here, the continuous decrease of the water permeance is mostly due to the increased thickness of the TpPa nanosheet layer, which gives rise to the increase in mass transfer resistance. Further, due to the electronegativity of carbonyl oxygen atoms in water,[40] we found that the surface of the TpPa membrane was negatively charged (Figure S19). Therefore, the separation can be ascribed to the combination of size-dependent sieving and electrostatic repulsion. As the long axis size of CR is as large as ~2.56 nm, the inherent channels of TpPa (~1.8 nm) can effectively reject them. Consequently, the membranes display pronounced CR rejections. As for AF with a long axis size of ~1.2 nm, it is

https://doi.org/10.1021/acs.chemmater.2c00834
Chem. Mater. 2022, 34, 6345−6354

reasonable that the TpPa membranes with a low deposition density exhibit a humble rejection. Fortunately, the increase of the deposition density is helpful to form overlapped structures to give a narrowed sieving size.[41] Together with the electrostatic repulsion, the thick TpPa nanosheet layers also give a remarkable AF removal efficiency. Moreover, the membrane structure remains intact after these filtration tests (Figure S20). We also deposited nanosheets of $TpBD(OH)_2$ on AAO supports by vacuum filtration and produced defect-free membranes. The separation performances of the $TpBD(OH)_2$ membranes were tested and shown in Figure S21. Similarly, the performance can be precisely tuned by adjusting the deposition density of $TpBD(OH)_2$ nanosheets. With a deposition density of 94 μg cm^{-2}, the membrane delivers a high water permeance of ~386 L m^{-2} h^{-1} bar^{-1}, while the rejections to CR and AF reach ~99.3 and ~82.0%, respectively.

The membranes constructed by these CONs possess excellent separation performances. To highlight the superiority of these CON membranes, the comparison in terms of water permeance and dye rejection is made with results shown in Figure 4f (the detailed information is given in Table S2). Obviously, the CON membranes prepared in this work outperform most state-of-the-art membranes prepared from different materials, including polyamide (PA), COFs, and other 2D materials. Compared with traditional nonporous nanosheets, nanoporous CONs as building materials can endow the resulting membranes with prominent porosities, providing rich and short mass transfer pathways for improved water permeance without sacrificing the selectivity (Figure 4g).

In the process of textile dyeing, different kinds of inorganic salts such as Na_2SO_4 and NaCl are extensively used as auxiliaries.[42] Processing streams containing both dyes and salts are thus frequently involved, which requires an effective desalination technique to separate salts from dyes for the sake of recycling of dyes and wastewater treatment.[43,44] In view of the high water permeances and prominent dye rejections, we expect that the TpPa membranes presented here may be competent for this challenging separation task. To confirm this, the rejections to three typical inorganic salts (Na_2SO_4, $MgSO_4$, and NaCl) with a concentration of 1000 ppm were tested. Figure S22 shows that all of these TpPa membranes exhibit low rejections to salts (<15%). The negligible salt removal efficiency can be ascribed to the passage of ions through the microporous TpPa layer, whose effective sieving size is far larger than the hydrated diameters of these salt ions but smaller than those of dye molecules. To verify the feasibility of practical applications, the performance durability of the TpPa membrane for dye/salt separation was accordingly investigated (Figure 4h). During the long-term filtration, the TpPa membrane presents a relatively stable dye rejection (>93%) and low salt rejection (<10%). Meanwhile, a moderate drop in water permeance occurs as the stacked nanosheets tend to be compacted under applied pressures, and the permeance remains stable after continuous filtration for ~17 h (Figure S23). The slightly reduced rejection to CR is mainly caused by the concentration polarization in the continuous dead-end operation. In general, the TpPa membranes show durable separation performances, demonstrating their great potential in highly efficient separation of dyes and salts.

4. CONCLUSIONS

In summary, we have developed a glycerol-mediated strategy to massively synthesize high-quality CONs with uniform thicknesses. The CONs are synthesized by simply mixing monomers predispersed in glycerol, followed by thermal treatment to initiate the condensation of intermediates. Owing to the strong hydrogen bonding interactions and high viscosity of glycerol, the $\pi-\pi$ stacking interactions between COF layers are effectively suppressed, leading to the direct formation of well-dispersed thin CONs with a high yield of >70%. The CON membranes are prepared on porous AAO substrates through vacuum filtration and exhibit uniform separation layers with tunable thicknesses. The prepared membranes show high water permeances and high dye rejections by virtue of ordered and charged pores in these CONs. Moreover, the membranes allow the penetration of salts, making them promising for the desalinization of dye wastewater. This work develops an unprecedented solvent-mediated strategy for the facile, efficient, and potentially up-scalable production of CONs and increases the understanding of the formation of 2D structures in the diffusion-controlled milieu.

■ ASSOCIATED CONTENT

Supporting Information

The Supporting Information is available free of charge at https://pubs.acs.org/doi/10.1021/acs.chemmater.2c00834.

Photographs; SEM images; AFM images; NMR spectra; mass spectra; membrane morphology; UV−vis adsorption spectra; detailed information of dyes; ζ potential curve; separation performance of the $TpBD(OH)_2$ membranes; performance comparison; salt rejections; and long-term filtration performance of TpPa membranes (PDF)

■ AUTHOR INFORMATION

Corresponding Authors

Xiansong Shi − *State Key Laboratory of Materials-Oriented Chemical Engineering, College of Chemical Engineering, Nanjing Tech University, Nanjing 211816, P. R. China;* orcid.org/0000-0002-4258-7941; Email: xsshi@njtech.edu.cn

Yong Wang − *State Key Laboratory of Materials-Oriented Chemical Engineering, College of Chemical Engineering, Nanjing Tech University, Nanjing 211816, P. R. China;* orcid.org/0000-0002-8653-514X; Email: yongwang@njtech.edu.cn

Authors

Zhipeng Zhang − *State Key Laboratory of Materials-Oriented Chemical Engineering, College of Chemical Engineering, Nanjing Tech University, Nanjing 211816, P. R. China*

Qianqian Lan − *State Key Laboratory of Materials-Oriented Chemical Engineering, College of Chemical Engineering, Nanjing Tech University, Nanjing 211816, P. R. China;* Present Address: Key Laboratory of Synthetic and Biological Colloids, Ministry of Education, School of Chemical and Material Engineering, Jiangnan University, Wuxi 214122, P. R. China; orcid.org/0000-0003-2602-6746

https://doi.org/10.1021/acs.chemmater.2c00834
Chem. Mater. 2022, 34, 6345−6354

Decai Liao − *State Key Laboratory of Materials-Oriented Chemical Engineering, College of Chemical Engineering, Nanjing Tech University, Nanjing 211816, P. R. China*
Mingjie Wei − *State Key Laboratory of Materials-Oriented Chemical Engineering, College of Chemical Engineering, Nanjing Tech University, Nanjing 211816, P. R. China;* orcid.org/0000-0001-7601-4749
Zhe Zhang − *State Key Laboratory of Materials-Oriented Chemical Engineering, College of Chemical Engineering, Nanjing Tech University, Nanjing 211816, P. R. China*
Xingyuan Wang − *State Key Laboratory of Materials-Oriented Chemical Engineering, College of Chemical Engineering, Nanjing Tech University, Nanjing 211816, P. R. China*

Complete contact information is available at: https://pubs.acs.org/10.1021/acs.chemmater.2c00834

Author Contributions

[§]Z.Z. and Q.L. contributed equally to this work.

Notes

The authors declare the following competing financial interest(s): Nanjing Tech University has filed the patent application related to the findings described in this manuscript.

■ ACKNOWLEDGMENTS

This work was financially supported by the National Natural Science Foundation of China (21825803). The authors also thank the High-Performance Computing Center at Nanjing Tech University for supporting the computational resource.

■ REFERENCES

(1) Cote, A. P.; Benin, A. I.; Ockwig, N. W.; O'Keeffe, M.; Matzger, A. J.; Yaghi, O. M. Porous, crystalline, covalent organic frameworks. *Science* **2005**, *310*, 1166−1170.
(2) Diercks, C. S.; Yaghi, O. M. The atom, the molecule, and the covalent organic framework. *Science* **2017**, *355*, No. eaal1585.
(3) Geng, K.; He, T.; Liu, R.; Dalapati, S.; Tan, K. T.; Li, Z.; Tao, S.; Gong, Y.; Jiang, Q.; Jiang, D. Covalent organic frameworks: design, synthesis, and functions. *Chem. Rev.* **2020**, *120*, 8814−8933.
(4) Rodríguez-San-Miguel, D.; Montoro, C.; Zamora, F. Covalent organic framework nanosheets: preparation, properties and applications. *Chem. Soc. Rev.* **2020**, *49*, 2291−2302.
(5) Ren, X.; Liao, G.; Li, Z.; Qiao, H.; Zhang, Y.; Yu, X.; Wang, B.; Tan, H.; Shi, L.; Qi, X.; Zhang, H. Two-dimensional MOF and COF nanosheets for next-generation optoelectronic applications. *Coord. Chem. Rev.* **2021**, *435*, No. 213781.
(6) Li, G.; Zhang, K.; Tsuru, T. Two-dimensional covalent organic framework (COF) membranes fabricated *via* the assembly of exfoliated COF nanosheets. *ACS Appl. Mater. Interfaces* **2017**, *9*, 8433−8436.
(7) Yang, H.; Yang, L.; Wang, H.; Xu, Z.; Zhao, Y.; Luo, Y.; Nasir, N.; Song, Y.; Wu, H.; Pan, F.; Jiang, Z. Covalent organic framework membranes through a mixed-dimensional assembly for molecular separations. *Nat. Commun.* **2019**, *10*, No. 2101.
(8) Luo, M.; Yang, Q.; Yang, W.; Wang, J.; He, F.; Liu, K.; Cao, H.; Yan, H. Defects engineering leads to enhanced photocatalytic H_2 evolution on graphitic carbon nitride-covalent organic framework nanosheet composite. *Small* **2020**, *16*, No. 2001100.
(9) Sun, M. H.; Huang, S. Z.; Chen, L. H.; Li, Y.; Yang, X. Y.; Yuan, Z. Y.; Su, B. L. Applications of hierarchically structured porous materials from energy storage and conversion, catalysis, photocatalysis, adsorption, separation, and sensing to biomedicine. *Chem. Soc. Rev.* **2016**, *45*, 3479−3563.
(10) Grill, L.; Dyer, M.; Lafferentz, L.; Persson, M.; Peters, M. V.; Hecht, S. Nano-architectures by covalent assembly of molecular building blocks. *Nat. Nanotechnol.* **2007**, *2*, 687−691.
(11) Berlanga, I.; Ruiz-Gonzalez, M. L.; Gonzalez-Calbet, J. M.; Fierro, J. L.; Mas-Balleste, R.; Zamora, F. Delamination of layered covalent organic frameworks. *Small* **2011**, *7*, 1207−1211.
(12) Chandra, S.; Kandambeth, S.; Biswal, B. P.; Lukose, B.; Kunjir, S. M.; Chaudhary, M.; Babarao, R.; Heine, T.; Banerjee, R. Chemically stable multilayered covalent organic nanosheets from covalent organic frameworks *via* mechanical delamination. *J. Am. Chem. Soc.* **2013**, *135*, 17853−17861.
(13) Yao, J.; Liu, C.; Liu, X.; Guo, J.; Zhang, S.; Zheng, J.; Li, S. Azobenzene-assisted exfoliation of 2D covalent organic frameworks into large-area, few-layer nanosheets for high flux and selective molecular separation membrane. *J. Membr. Sci.* **2020**, *601*, No. 117864.
(14) Liu, W.; Li, X.; Wang, C.; Pan, H.; Liu, W.; Wang, K.; Zeng, Q.; Wang, R.; Jiang, J. A scalable general synthetic approach toward ultrathin imine-linked two-dimensional covalent organic framework nanosheets for photocatalytic CO_2 reduction. *J. Am. Chem. Soc.* **2019**, *141*, 17431−17440.
(15) Shi, X.; Ma, D.; Xu, F.; Zhang, Z.; Wang, Y. Table-salt enabled interface-confined synthesis of covalent organic framework (COF) nanosheets. *Chem. Sci.* **2020**, *11*, 989−996.
(16) Dey, K.; Mohata, S.; Banerjee, R. Covalent organic frameworks and supramolecular nano-synthesis. *ACS Nano* **2021**, *15*, 12723−12740.
(17) Yang, L. X.; Zhu, Y. J.; Tong, H.; Liang, Z. H.; Wang, W. W. Hierarchical beta-$Ni(OH)_2$ and NiO carnations assembled from nanosheet building blocks. *Cryst. Growth Des.* **2007**, *7*, 2716−2719.
(18) Hu, J.; Weng, S.; Zheng, Z.; Pei, Z.; Huang, M.; Liu, P. Solvents mediated-synthesis of BiOI photocatalysts with tunable morphologies and their visible-light driven photocatalytic performances in removing of arsenic from water. *J. Hazard. Mater.* **2014**, *264*, 293−302.
(19) Wang, B.; Chen, J. S.; Wang, Z.; Madhavi, S.; Lou, X. W. D. Green synthesis of NiO nanobelts with exceptional pseudo-capacitive properties. *Adv. Energy Mater.* **2012**, *2*, 1188−1192.
(20) Lan, K.; Liu, Y.; Zhang, W.; Liu, Y.; Elzatahry, A.; Wang, R.; Xia, Y.; Al-Dhayan, D.; Zheng, N.; Zhao, D. Uniform ordered two-dimensional mesoporous TiO_2 nanosheets from hydrothermal-induced solvent-confined monomicelle assembly. *J. Am. Chem. Soc.* **2018**, *140*, 4135−4143.
(21) Lan, Q. Q.; Zhang, Z. P.; Xu, F.; Wei, M. J.; Wang, Y. Nanomeshes with sub-10 nm pores by glycerol-triggered 2D assembly in liquid phases for fast and selective membranes. *Nano Lett.* **2021**, *21*, 3302−3309.
(22) Sun, H.; Mumby, S. J.; Maple, J. R.; Hagler, A. T. An ab-initio CFF93 all-atom force field for polycarbonates. *J. Am. Chem. Soc.* **1994**, *116*, 2978−2987.
(23) Zhang, F. M.; Sheng, J. L.; Yang, Z. D.; Sun, X. J.; Tang, H. L.; Lu, M.; Dong, H.; Shen, F. C.; Liu, J.; Lan, Y. Q. Rational design of MOF/COF hybrid materials for photocatalytic H2 evolution in the presence of sacrificial electron donors. *Angew. Chem., Int. Ed.* **2018**, *57*, 12106−12110.
(24) Kandambeth, S.; Mallick, A.; Lukose, B.; Mane, M. V.; Heine, T.; Banerjee, R. Construction of crystalline 2D covalent organic frameworks with remarkable chemical (acid/base) stability *via* a combined reversible and irreversible route. *J. Am. Chem. Soc.* **2012**, *134*, 19524−19527.
(25) Wang, R.; Shi, X.; Xiao, A.; Zhou, W.; Wang, Y. Interfacial polymerization of covalent organic frameworks (COFs) on polymeric substrates for molecular separations. *J. Membr. Sci.* **2018**, *566*, 197−204.
(26) Pachfule, P.; Kandmabeth, S.; Mallick, A.; Banerjee, R. Hollow tubular porous covalent organic framework (COF) nanostructures. *Chem. Commun.* **2015**, *51*, 11717−11720.
(27) Showler, A. J.; Darley, P. A. Condensation products of glycerol with aldehydes and ketones. 2-Substituted m-dioxan-5-ols and 1,3-dioxolane-4-methanols. *Chem. Rev.* **1967**, *67*, 427−440.
(28) Yamamoto, K.; Kiyan, A. M.; Bagio, J. C.; Rossi, K. A. B.; Delabio Berezuk, F.; Berezuk, M. E. Green cyclic acetals production

by glycerol etherification reaction with benzaldehyde using cationic acidic resin. *Green Process. Synth.* **2019**, *8*, 183−190.
(29) Irvine, J. C.; Macdonald, J. L. A.; Soutar, C. W. XXXIX.—Condensation of acetone and benzaldehyde with glycerol. Preparation of glycerol α-methyl ether. *J. Chem. Soc., Trans.* **1915**, *107*, 337−351.
(30) Guo, Z.; Jiang, H.; Wu, H.; Zhang, L.; Song, S.; Chen, Y.; Zheng, C.; Ren, Y.; Zhao, R.; Li, Y.; Yin, Y.; Guiver, M. D.; Jiang, Z. Oil-water-oil triphase synthesis of ionic covalent organic framework nanosheets. *Angew. Chem., Int. Ed.* **2021**, *60*, 27078−27085.
(31) Biswal, B. P.; Chandra, S.; Kandambeth, S.; Lukose, B.; Heine, T.; Banerjee, R. Mechanochemical synthesis of chemically stable isoreticular covalent organic frameworks. *J. Am. Chem. Soc.* **2013**, *135*, 5328−5331.
(32) Chandra, S.; Roy Chowdhury, D.; Addicoat, M.; Heine, T.; Paul, A.; Banerjee, R. Molecular level control of the capacitance of two-dimensional covalent organic frameworks: role of hydrogen bonding in energy storage materials. *Chem. Mater.* **2017**, *29*, 2074−2080.
(33) Ding, S. Y.; Gao, J.; Wang, Q.; Zhang, Y.; Song, W. G.; Su, C. Y.; Wang, W. Construction of covalent organic framework for catalysis: Pd/COF-LZU1 in Suzuki-Miyaura coupling reaction. *J. Am. Chem. Soc.* **2011**, *133*, 19816−19822.
(34) Li, Z.; Feng, X.; Zou, Y.; Zhang, Y.; Xia, H.; Liu, X.; Mu, Y. A 2D azine-linked covalent organic framework for gas storage applications. *Chem. Commun.* **2014**, *50*, 13825−13828.
(35) Prozorovska, L.; Kidambi, P. R. State-of-the-art and future prospects for atomically thin membranes from 2D materials. *Adv. Mater.* **2018**, *30*, No. 1801179.
(36) Liu, G.; Jin, W.; Xu, N. Two-dimensional-material membranes: A new family of high-performance separation membranes. *Angew. Chem., Int. Ed.* **2016**, *55*, 13384−13397.
(37) Ding, L.; Wei, Y.; Wang, Y.; Chen, H.; Caro, J.; Wang, H. A two-dimensional lamellar membrane: MXene nanosheet stacks. *Angew. Chem., Int. Ed.* **2017**, *56*, 1825−1829.
(38) Shinde, D. B.; Sheng, G.; Li, X.; Ostwal, M.; Emwas, A. H.; Huang, K. W.; Lai, Z. Crystalline 2D covalent organic framework membranes for high-flux organic solvent nanofiltration. *J. Am. Chem. Soc.* **2018**, *140*, 14342−14349.
(39) Shi, X.; Zhang, Z.; Fang, S.; Wang, J.; Zhang, Y.; Wang, Y. Flexible and robust three-dimensional covalent organic framework membranes for precise separations under extreme conditions. *Nano Lett.* **2021**, *21*, 8355−8362.
(40) Xu, F.; Wang, Y. X.; Lian, C.; Xu, Z. Fast proton-selective transport through covalent organic frameworks in aqueous phase. *J. Membr. Sci.* **2022**, *648*, No. 120361.
(41) Yin, C.; Zhang, Z.; Zhou, J.; Wang, Y. Single-layered nanosheets of covalent triazine frameworks (CTFs) by mild oxidation for molecular-sieving membranes. *ACS Appl. Mater. Interfaces* **2020**, *12*, 18944−18951.
(42) Holkar, C. R.; Jadhav, A. J.; Pinjari, D. V.; Mahamuni, N. M.; Pandit, A. B. A critical review on textile wastewater treatments: Possible approaches. *J. Environ. Manage.* **2016**, *182*, 351−366.
(43) Tavangar, T.; Karimi, M.; Rezakazemi, M.; Reddy, K. R.; Aminabhavi, T. M. Textile waste, dyes/inorganic salts separation of cerium oxide-loaded loose nanofiltration polyethersulfone membranes. *Chem. Eng. J.* **2020**, *385*, No. 123787.
(44) Lin, J.; Ye, W.; Zeng, H.; Yang, H.; Shen, J.; Darvishmanesh, S.; Luis, P.; Sotto, A.; Van der Bruggen, B. Fractionation of direct dyes and salts in aqueous solution using loose nanofiltration membranes. *J. Membr. Sci.* **2015**, *477*, 183−193.

NOTE ADDED AFTER ASAP PUBLICATION

This paper was published ASAP on July 14, 2022. Additional changes were made to the equation on page two, and the corrected version was reposted on July 15, 2022.

https://doi.org/10.1021/acs.chemmater.2c00834
Chem. Mater. 2022, 34, 6345−6354